High-order integral equation methods for problems of scattering by bumps and cavities on half-planes

Carlos Pérez-Arancibia and Oscar P. Bruno*

Computing & Mathematical Sciences, California Institute of Technology, 1200 E. California Blvd., Pasadena, California 91125, USA
**Corresponding author: obruno@caltech.edu*

Received May 19, 2014; accepted June 17, 2014;
posted June 20, 2014 (Doc. ID 212305); published July 15, 2014

This paper presents high-order integral equation methods for the evaluation of electromagnetic wave scattering by dielectric bumps and dielectric cavities on perfectly conducting or dielectric half-planes. In detail, the algorithms introduced in this paper apply to eight classical scattering problems, namely, scattering by a dielectric bump on a perfectly conducting or a dielectric half-plane, and scattering by a filled, overfilled, or void dielectric cavity on a perfectly conducting or a dielectric half-plane. In all cases field representations based on single-layer potentials for appropriately chosen Green functions are used. The numerical *far fields and near fields* exhibit excellent convergence as discretizations are refined—even at and around points where singular fields and infinite currents exist.

OCIS codes: (000.4430) Numerical approximation and analysis; (240.3695) Linear and nonlinear light scattering from surfaces; (290.1350) Backscattering; (290.5880) Scattering, rough surfaces.
http://dx.doi.org/10.1364/JOSAA.31.001738

1. INTRODUCTION

This paper presents high-order integral equation methods for the numerical solution of problems of scattering of a plane electromagnetic wave by cylindrical dielectric defects at the interface between two half-planes. Eight such classical problems are tackled in this contribution: scattering by a dielectric bump on (1) a perfectly electrically conducting (PEC) or (2) a dielectric half-plane [Fig. 1(a)]; scattering by a dielectric-filled cavity on (3) a perfectly conducting or (4) a dielectric half-plane [Fig. 1(b)]; scattering by a dielectric-overfilled cavity on (5) a perfectly conducting or (6) a dielectric half-plane [Fig. 1(c)]; and scattering by a void cavity on (7) a perfectly conducting or (8) a dielectric half-plane [Fig. 1(d)]. From a mathematical perspective these eight different physical problems reduce to just three problem types for which this paper provides numerical solutions on the basis of highly accurate and efficient boundary integral equation methods.

In all cases the proposed methods utilize field representations based on single-layer potentials for appropriately chosen Green functions. As is known, such single-layer formulations lead to noninvertible integral equations at certain spurious resonances—that is, for wavenumbers that coincide with interior Dirichlet eigenvalues for a certain differential operator—either the Laplace operator or an elliptic differential operator with piecewise constant coefficients (see Section 4.B for details). We nevertheless show that solutions *for all wavenumbers* can be obtained from such noninvertible formulations—including wavenumbers at which noninvertible integral equations result. Our method in these regards relies on the analyticity of the PDE solution as a function of the wavenumber together with a certain approach based on use of Chebyshev approximation.

(The use of field representations that give rise to noninvertible operators is advantageous in two main ways: on one hand this strategy allows one to bypass the need to utilize hypersingular operators, whose evaluation is computationally expensive and, otherwise, highly challenging near corner points; and, on the other hand, it leads to systems of integral equations containing fewer integral operators—with associated reduced computational cost.)

The problems considered in this paper draw considerable interest in a wide range of settings. For example, the problem of scattering by bumps and cavities on a (perfect or imperfect) conducting half-plane is important in the study of the radio-frequency absorption and electric and magnetic field enhancement that arise from surface roughness [1,2]. The problem of scattering by open groove cavities on a conducting plane, in turn, impacts on a variety of technologies, with applicability to the design of cavity-backed antennas, nondestructive evaluation of material surfaces, and more recently, modeling of extraordinary transmission of light and plasmonics resonance, amongst many others (e.g., [3] and references therein).

There is vast literature concerning the types of problems considered in this paper. For a circular bump a separation-of-variables analytical Fourier–Bessel expansion exists [4]. Related semianalytical separation-of-variables solutions are available for other simple configurations, such as semicircular cavities and rectangular bumps and cavities (e.g., [5–12] and references therein), while solutions based on Fourier-type integral representations, mode matching techniques, and staircase approximation of the geometry are available for more general domains (e.g., [13] and references therein). Even for simple configurations, such as a circular cavity or bump on a perfectly conducting plane, the semianalytical separation-of-variables method requires solution of an infinite

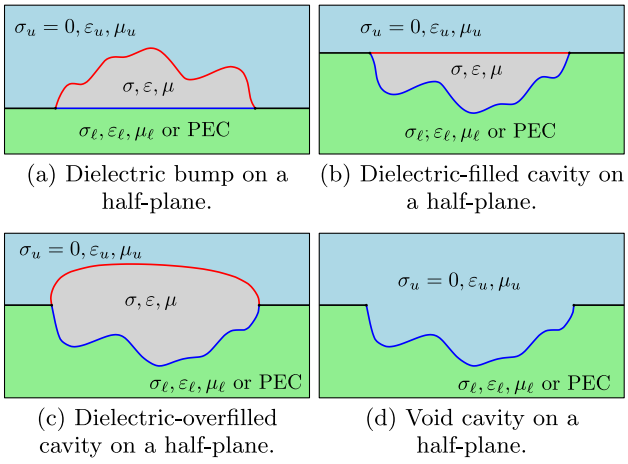

(a) Dielectric bump on a half-plane. (b) Dielectric-filled cavity on a half-plane. (c) Dielectric-overfilled cavity on a half-plane. (d) Void cavity on a half-plane.

Fig. 1. Schematics of the eight physical problems considered in this paper.

dimensional linear system of equations that must be truncated to an $n \times n$ system and solved numerically [9,14,15,10,11]. As it happens, the resulting (full) matrix is extremely ill-conditioned for large values of n. In practice only limited accuracy results from use of such algorithms: use of small values of n naturally produces limited accuracy, while for large values of the n matrix ill-conditioning arises as an accuracy limiting element.

Finite element and finite difference methods of low order of accuracy have been used extensively over the last decade [3,16–22]. As is well known, finite element and finite difference methods lead to sparse linear systems. However, in order to satisfy the Sommerfeld radiation condition at infinity, a relatively large computational domain containing the scatterer must be utilized (unless a nonlocal boundary condition is used, with a consequent loss of sparsity). In view of the large required computational domains (or large coupled systems of equations for methods that use nonlocal domain truncation) and their low-order convergence (especially around corners where fields are singular and currents are infinite), these methods yield very slow convergence, and, therefore, for adequately accurate solutions, they require use of large numbers of unknowns and a high computational cost.

Boundary integral equation methods [whose best known representative in the engineering literature is the *method of moments* (MoM)], on the other hand, lead to linear systems of reduced dimensionality, the associated solutions automatically satisfy the condition of radiation at infinity, and, unlike finite element methods, they do not suffer from dispersion errors. Integral/MoM approaches have been used previously for the solution of the problem of scattering by an empty and dielectric-filled cavity on a perfectly conducting half-plane; see, e.g., [23–25]. However, previous integral/MoM approaches for these problems are based on the use of low-order numerical algorithms, and, most importantly, they do not accurately account for singular field behavior at corners—and, thus, they may not be sufficiently accurate for evaluation of important physical mechanisms that arise from singular electrical currents and local fields at and around corners. While the high-order methods presented in this paper are based on Nyström (collocation) sampling, a high-order MoM (Galerkin) testing strategy could be implemented (albeit at higher computational cost) on the basis of the same set of ideas.

This paper is organized as follows. Section 2 presents a brief description of the various problems at hand, and Section 3 introduces a new set of integral equations for their treatment. Section 4 then describes the high-order solvers we have developed for the numerical solution of these integral equations, which include full resolution of singular fields at corners. The excellent convergence properties of the equations and algorithms introduced in this text are demonstrated in Section 5. In particular, the high accuracy of the new methods in the presence of corner singularities can be used to evaluate the effects of corner singularities on currents and local fields on and around bumps and cavities, and, thus, on important physical observables, such as absorption, extraordinary transmission, and cavity resonance.

2. SCATTERING PROBLEM

All the problems considered in this contribution can be described mathematically following the compact depiction presented in Fig. 2. Thus, a plane wave $\mathbf{H}^{\text{inc}}(\boldsymbol{x}) = \mathbf{H}^0 e^{i\mathbf{k}\cdot\boldsymbol{x}}$, $\mathbf{E}^{\text{inc}}(\boldsymbol{x}) = \mathbf{E}^0 e^{i\mathbf{k}\cdot\boldsymbol{x}}$ with wave vector $\mathbf{k} = k_3(\cos\alpha, \sin\alpha)$ impinges on a cavity formed by the subdomains Ω_1 and Ω_2, which lies on the boundary of an otherwise planar horizontal interface between the infinite subdomains Ω_3 and Ω_4. As is well known, the z components $u = E_z$ and $u = H_z$ of the total electric and magnetic fields satisfy the Helmholtz equation

$$\Delta u + k_j^2 u = 0 \quad \text{in} \quad \Omega_j, \tag{1}$$

where, letting $\omega > 0$, $\varepsilon_j > 0$, $\mu_j > 0$, and $\sigma_j \geq 0$ denote the angular frequency, the electric permittivity, the magnetic permeability, and the electrical conductivity, the wavenumber k_j ($\Im(k_j) > 0$) is defined by $k_j^2 = \omega^2(\varepsilon_j + i\sigma_j/\omega)\mu_j$, $1 \leq j \leq 4$. Throughout this paper it is assumed that Ω_3 is a lossless medium ($\sigma_3 = 0$).

In order to formulate transmission problems for the transverse components of the electromagnetic field, u is expressed as

$$u = \begin{cases} u_1 & \text{in} \quad \Omega_1, \\ u_2 & \text{in} \quad \Omega_2, \\ u_3 + f & \text{in} \quad \Omega_3, \\ u_4 + f & \text{in} \quad \Omega_4, \end{cases} \tag{2}$$

where f is the solution (presented below in this section) of the problem of scattering by the lower half-plane *in absence of the dielectric defect* (see [26] for details).

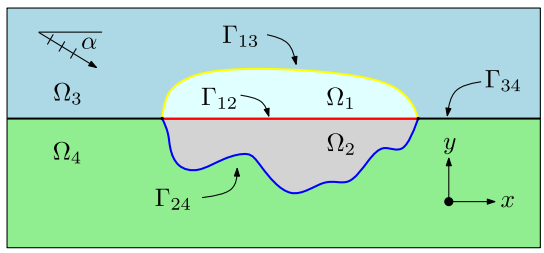

Fig. 2. Compact mathematical description of the problems considered in this paper.

Additionally, u satisfies the transmission conditions

$$u_i - u_j = g, \qquad \frac{1}{\beta_i}\frac{\partial u_i}{\partial \mathbf{n}} - \frac{1}{\beta_j}\frac{\partial u_j}{\partial \mathbf{n}} = \frac{1}{\beta_j}\frac{\partial g}{\partial \mathbf{n}}, \tag{3}$$

at the interface Γ_{ij} between Ω_i and Ω_j, where $\beta_j = \mu_j$ in TM polarization and $\beta_j = \varepsilon_j + i\sigma_j/\omega$ in TE polarization. For each one of the problems considered in this paper Eqs. (3) with $g = f$ are satisfied on Γ_{13}. In the case in which Ω_4 is filled by a dielectric material the transmission conditions (3) are also satisfied with boundary data $g = f$ on Γ_{24}, and they are satisfied with boundary data $g = 0$ on Γ_{34}. On the other hand, when Ω_4 is a perfectly conducting half-plane, $u_4 = 0$ and boundary conditions

$$u_j = 0 \quad \text{and} \quad \frac{\partial u_j}{\partial \mathbf{n}} = 0, \qquad j = 2,3 \tag{4}$$

are satisfied on Γ_{j4} in TM and TE polarization, respectively. Additionally, the scattering fields u_j, $j = 3,4$ fulfill the Sommerfeld radiation condition at infinity.

3. INTEGRAL EQUATION FORMULATIONS

Three main problem types can be identified in connection with Fig. 2, namely *Problem Type I*, where transmission conditions (3) are imposed on Γ_{13} and Γ_{24} (which, in our context, characterize the problem of scattering by a dielectric bump on a dielectric half-plane as well as the problems of scattering by a filled, overfilled, or empty cavity on a dielectric half-plane); *Problem Type II*, where transmission conditions (3) are imposed on Γ_{13} and PEC boundary condition (4) is imposed on Γ_{24}, which applies to the problem of scattering by a (filled, overfilled, or empty) cavity on a PEC half-plane; and *Problem Type III*, where transmission conditions (3) are only imposed on Γ_{13}, with application to the problem of scattering by a dielectric bump on a perfectly conducting half-plane. In the following three sections we derive systems of boundary integral equations for each one of these problem types.

A. Problem Type I

In Problem Type I the domains Ω_j $(1 \le j \le 4)$ contain dielectric media of finite or zero conductivity; we denote by k_j the (real or complex) wavenumber in the domain Ω_j. Note the following:

– For the problem of scattering by a *dielectric-filled cavity on a dielectric half-plane* we have $k_3 = k_1, k_1 \neq k_2, k_2 \neq k_4$;
– For the problem of scattering by an *overfilled cavity on a dielectric half-plane* we have $k_3 \neq k_1, k_1 = k_2, k_2 \neq k_4$; and
– For the problem of scattering by a *void cavity on a dielectric half-plane* we have $k_3 = k_1, k_1 = k_2, k_2 \neq k_4$.

To tackle the Type I problem we express the total field u by means the single-layer-potential representation

$$u = \begin{cases} \mathcal{S}_{\text{int}}[\psi_{\text{int}}] & \text{in} \quad \Omega_1 \cup \Omega_2, \\ \mathcal{S}_{\text{ext}}[\psi_{\text{ext}}] + f & \text{in} \quad \Omega_3 \cup \Omega_4, \end{cases} \tag{5}$$

in terms of the unknown density functions ψ_{int} and ψ_{ext}, where, letting $G_{k_j}^{k_i}$ denote the Green function of the Helmholtz equation for the two-layer medium with wavenumbers k_i and k_j in the upper and lower half-planes, respectively (see [26]), we have set

$$\mathcal{S}_{\text{int}}[\psi](\boldsymbol{x}) = \int_{\Gamma_{13}\cup\Gamma_{24}} G_{k_2}^{k_1}(\boldsymbol{x},\boldsymbol{y})\psi(\boldsymbol{y})\mathrm{d}s_{\boldsymbol{y}}, \tag{6a}$$

$$\mathcal{S}_{\text{ext}}[\psi](\boldsymbol{x}) = \int_{\Gamma_{13}\cup\Gamma_{24}} G_{k_4}^{k_3}(\boldsymbol{x},\boldsymbol{y})\psi(\boldsymbol{y})\mathrm{d}s_{\boldsymbol{y}}. \tag{6b}$$

The Green functions $G_{k_j}^{k_i}$ satisfy the transmission conditions (3) on Γ_{ij} [with (ij) equal to either Eq. (12) or Eq. (34)], and, therefore, they depend on the polarization (through the parameters β_i and β_j). Note, further, that for $k_i = k_j = k$ the Green function $G_{k_j}^{k_i}$ equals the free-space Green function with wavenumber k.

It is easy to check that the representation (5) for the solution u satisfies the Helmholtz equation with wavenumber k_j in the domain Ω_j $(1 \le j \le 4)$ as well as the radiation conditions at infinity. Since the two-layer Green functions satisfy the relevant transmission conditions on Γ_{12} and Γ_{34}, there remain only two boundary conditions to be satisfied, namely, the transmission conditions (3) on the boundary of the defect $\Omega_1 \cup \Omega_2$. Using classical jump relations [27] for various layer potentials, these conditions lead to the system

$$\begin{aligned} S_{\text{int}}^{\Gamma_{13}}[\psi_{\text{int}}] - S_{\text{ext}}^{\Gamma_{13}}[\psi_{\text{ext}}] &= f, \\ \frac{\beta_3}{\beta_1}\left\{\frac{\psi_{\text{int}}}{2} + K_{\text{int}}^{\Gamma_{13}}[\psi_{\text{int}}]\right\} + \frac{\psi_{\text{ext}}}{2} - K_{\text{ext}}^{\Gamma_{13}}[\psi_{\text{ext}}] &= \frac{\partial f}{\partial \mathbf{n}}, \\ S_{\text{int}}^{\Gamma_{24}}[\psi_{\text{int}}] - S_{\text{ext}}^{\Gamma_{24}}[\psi_{\text{ext}}] &= f, \\ \frac{\beta_4}{\beta_2}\left\{\frac{\psi_{\text{int}}}{2} + K_{\text{int}}^{\Gamma_{24}}[\psi_{\text{int}}]\right\} + \frac{\psi_{\text{ext}}}{2} - K_{\text{ext}}^{\Gamma_{24}}[\psi_{\text{ext}}] &= \frac{\partial f}{\partial \mathbf{n}} \end{aligned} \tag{7}$$

of boundary integral equations on the open curves Γ_{13} and Γ_{24} for the unknowns ψ_{int} and ψ_{ext}. The boundary integral operators in Eq. (7) for $(ij) = (13)$ and $(ij) = (24)$ are given by

$$\begin{aligned} S_{\text{int}}^{\Gamma_{ij}}[\psi](\boldsymbol{x}) &= \int_{\Gamma_{13}\cup\Gamma_{24}} G_{k_2}^{k_1}(\boldsymbol{x},\boldsymbol{y})\psi(\boldsymbol{y})\mathrm{d}s_{\boldsymbol{y}}, \qquad \boldsymbol{x} \in \Gamma_{ij}, \\ S_{\text{ext}}^{\Gamma_{ij}}[\psi](\boldsymbol{x}) &= \int_{\Gamma_{13}\cup\Gamma_{24}} G_{k_4}^{k_3}(\boldsymbol{x},\boldsymbol{y})\psi(\boldsymbol{y})\mathrm{d}s_{\boldsymbol{y}}, \qquad \boldsymbol{x} \in \Gamma_{ij}, \\ K_{\text{int}}^{\Gamma_{ij}}[\psi](\boldsymbol{x}) &= \int_{\Gamma_{13}\cup\Gamma_{24}} \frac{\partial G_{k_2}^{k_1}}{\partial \mathbf{n}_{\boldsymbol{x}}}(\boldsymbol{x},\boldsymbol{y})\psi(\boldsymbol{y})\mathrm{d}s_{\boldsymbol{y}}, \qquad \boldsymbol{x} \in \Gamma_{ij}, \\ K_{\text{ext}}^{\Gamma_{ij}}[\psi](\boldsymbol{x}) &= \int_{\Gamma_{13}\cup\Gamma_{24}} \frac{\partial G_{k_4}^{k_3}}{\partial \mathbf{n}_{\boldsymbol{x}}}(\boldsymbol{x},\boldsymbol{y})\psi(\boldsymbol{y})\mathrm{d}s_{\boldsymbol{y}}, \qquad \boldsymbol{x} \in \Gamma_{ij}. \end{aligned} \tag{8}$$

B. Problem Type II

In Problem Type II the domain Ω_4 contains a PEC medium, and the domains Ω_j $(1 \le j \le 3)$ contain dielectric media of finite or zero conductivity; we denote by k_j the (real or complex) wavenumber in the domain Ω_j $(1 \le j \le 3)$. Clearly,

– For the problem of scattering by a *dielectric-filled cavity on a PEC half-plane* we have $k_3 = k_1, k_1 \neq k_2$;
– For the problem of scattering by an *overfilled cavity on a PEC half-plane* we have $k_3 \neq k_1, k_1 = k_2$; and
– For the problem of scattering by a *void cavity on a PEC half-plane* we have $k_3 = k_1, k_1 = k_2$.

For Type II problems we express the total field u by means of the single-layer-potential representation

$$u = \begin{cases} \mathcal{S}_{\rm int}[\psi_{\rm int}] & \text{in} \quad \Omega_1 \cup \Omega_2, \\ \mathcal{S}_{\rm ext}[\psi_{\rm ext}] + f & \text{in} \quad \Omega_3, \\ 0 & \text{in} \quad \Omega_4, \end{cases} \tag{9}$$

where, defining $G^{k_1}_{k_2}$ as in Section 3.A and letting $G^{k_3}_{\infty}$ denote the Green function that satisfies the PEC boundary condition (4) on Γ_{34}, the potentials above are defined by

$$\mathcal{S}_{\rm int}[\psi](\boldsymbol{x}) = \int_{\Gamma_{13}\cup\Gamma_{24}} G^{k_1}_{k_2}(\boldsymbol{x},\boldsymbol{y})\psi(\boldsymbol{y})\mathrm{d}s_{\boldsymbol{y}}, \tag{10a}$$

$$\mathcal{S}_{\rm ext}[\psi](\boldsymbol{x}) = \int_{\Gamma_{13}} G^{k_3}_{\infty}(\boldsymbol{x},\boldsymbol{y})\psi(\boldsymbol{y})\mathrm{d}s_{\boldsymbol{y}}. \tag{10b}$$

As mentioned in Section 3.A, the Green function $G^{k_i}_{k_j}$ depends on the polarization; the same is of course true for $G^{k_3}_{\infty}$, which is given by $G^{k}_{\infty}(\boldsymbol{x},\boldsymbol{y}) = G_k(\boldsymbol{x},\boldsymbol{y}) - G_k(\bar{\boldsymbol{x}},\boldsymbol{y})$ in TM polarization, and $G^{k}_{\infty}(\boldsymbol{x},\boldsymbol{y}) = G_k(\boldsymbol{x},\boldsymbol{y}) + G_k(\bar{\boldsymbol{x}},\boldsymbol{y})$ in TE polarization, where $\bar{\boldsymbol{x}} = (x_1, -x_2)$ and where $G_k(\boldsymbol{x},\boldsymbol{y}) = iH^{(1)}_0(k|\boldsymbol{x}-\boldsymbol{y}|)/4$ is the free-space Green function. By virtue of the integral representation (9) the field satisfies the Helmholtz equation in the domain Ω_j with wavenumber k_j $(1 \le j \le 3)$, the radiation condition at infinity, transmission conditions on Γ_{12}, and the PEC boundary conditions on Γ_{24}. Imposing the remaining transmission conditions (3) on Γ_{13} and PEC boundary condition (4) of Γ_{24}, we obtain the equations

$$\begin{aligned} S^{\Gamma_{13}}_{\rm int}[\psi_{\rm int}] - S^{\Gamma_{13}}_{\rm ext}[\psi_{\rm ext}] &= f, \\ \frac{\beta_3}{\beta_1}\left\{\frac{\psi_{\rm int}}{2} + K^{\Gamma_{13}}_{\rm int}[\psi_{\rm int}]\right\} + \frac{\psi_{\rm ext}}{2} - K^{\Gamma_{13}}_{\rm ext}[\psi_{\rm ext}] &= \frac{\partial f}{\partial \mathbf{n}}, \end{aligned} \tag{11a}$$

on Γ_{13} (valid for both TE and TM polarizations provided the corresponding constants β_j and Green functions are used) and

$$\frac{\psi_{\rm int}}{2} + K^{\Gamma_{24}}_{\rm int}[\psi_{\rm int}] = 0 \quad \text{(TE polarization)}, \tag{11b}$$

$$S^{\Gamma_{24}}_{\rm int}[\psi_{\rm int}] = 0 \quad \text{(TM polarization)} \tag{11c}$$

on Γ_{24}. In accordance with the definition of the single-layer potentials (10), the boundary integral operators in (11) for $(ij) = (13)$ and $(ij) = (24)$ are given by

$$\begin{aligned} S^{\Gamma_{ij}}_{\rm int}[\psi](\boldsymbol{x}) &= \int_{\Gamma_{13}\cup\Gamma_{24}} G^{k_1}_{k_2}(\boldsymbol{x},\boldsymbol{y})\psi(\boldsymbol{y})\mathrm{d}s_{\boldsymbol{y}}, \qquad \boldsymbol{x}\in\Gamma_{ij}, \\ S^{\Gamma_{ij}}_{\rm ext}[\psi](\boldsymbol{x}) &= \int_{\Gamma_{13}} G^{k_3}_{\infty}(\boldsymbol{x},\boldsymbol{y})\psi(\boldsymbol{y})\mathrm{d}s_{\boldsymbol{y}}, \qquad \boldsymbol{x}\in\Gamma_{ij}, \\ K^{\Gamma_{ij}}_{\rm int}[\psi](\boldsymbol{x}) &= \int_{\Gamma_{13}\cup\Gamma_{24}} \frac{\partial G^{k_1}_{k_2}}{\partial \mathbf{n}_{\boldsymbol{x}}}(\boldsymbol{x},\boldsymbol{y})\psi(\boldsymbol{y})\mathrm{d}s_{\boldsymbol{y}}, \qquad \boldsymbol{x}\in\Gamma_{ij}, \\ K^{\Gamma_{ij}}_{\rm ext}[\psi](\boldsymbol{x}) &= \int_{\Gamma_{13}} \frac{\partial G^{k_3}_{\infty}}{\partial \mathbf{n}_{\boldsymbol{x}}}(\boldsymbol{x},\boldsymbol{y})\psi(\boldsymbol{y})\mathrm{d}s_{\boldsymbol{y}}, \qquad \boldsymbol{x}\in\Gamma_{ij}. \end{aligned} \tag{12}$$

C. Problem Type III

For Problem Type III the domains Ω_j $(j = 1, 3)$ contain dielectric media of finite or zero conductivity (the corresponding, possibly complex, wavenumbers are denoted by k_1 and k_3), and the domains Ω_j, $j = 2, 4$, contain a PEC medium. Note the following:

– For the problem of scattering by a *dielectric bump on a PEC half-plane* we have $k_3 \neq k_1$.

As in the previous cases, for Type III problems the total field u is expressed by means of the single-layer-potential representation

$$u = \begin{cases} \mathcal{S}_{\rm int}[\psi_{\rm int}] & \text{in} \quad \Omega_1, \\ \mathcal{S}_{\rm ext}[\psi_{\rm ext}] + f & \text{in} \quad \Omega_3, \\ 0 & \text{in} \quad \Omega_2 \cup \Omega_4, \end{cases} \tag{13}$$

where the potentials above are defined by

$$\mathcal{S}_{\rm int}[\psi](\boldsymbol{x}) = \int_{\Gamma_{13}} G^{k_1}_{\infty}(\boldsymbol{x},\boldsymbol{y})\psi(\boldsymbol{y})\mathrm{d}s_{\boldsymbol{y}}, \tag{14a}$$

$$\mathcal{S}_{\rm ext}[\psi](\boldsymbol{x}) = \int_{\Gamma_{13}} G^{k_3}_{\infty}(\boldsymbol{x},\boldsymbol{y})\psi(\boldsymbol{y})\mathrm{d}s_{\boldsymbol{y}}. \tag{14b}$$

As mentioned in Section 3.B, the Green functions $G^{k_1}_{\infty}$ and $G^{k_3}_{\infty}$ depend on the polarization and satisfy the PEC boundary condition on Γ_{12} and Γ_{34}, respectively. The total field, as given by the potentials (14), satisfies Helmholtz equations with wavenumber k_j in the domain Ω_j, $j = 1, 3$, the PEC boundary condition on Γ_{24} and Γ_{12}, as well as the radiation condition at infinity. Imposing the transmission conditions (3) on Γ_{13}, the following system of boundary integral equations is obtained for the unknown density functions $\psi_{\rm int}$ and $\psi_{\rm ext}$:

$$\begin{aligned} S^{\Gamma_{13}}_{\rm int}[\psi_{\rm int}] - S^{\Gamma_{13}}_{\rm ext}[\psi_{\rm ext}] &= f, \\ \frac{\beta_3}{\beta_1}\left\{\frac{\psi_{\rm int}}{2} + K^{\Gamma_{13}}_{\rm int}[\psi_{\rm int}]\right\} + \frac{\psi_{\rm ext}}{2} - K^{\Gamma_{13}}_{\rm ext}[\psi_{\rm ext}] &= \frac{\partial f}{\partial \mathbf{n}}, \end{aligned} \tag{15}$$

on Γ_{13}, where the boundary integral operators are defined by

$$\begin{aligned} S^{\Gamma_{13}}_{\rm int}[\psi](\boldsymbol{x}) &= \int_{\Gamma_{13}} G^{k_1}_{\infty}(\boldsymbol{x},\boldsymbol{y})\psi(\boldsymbol{y})\mathrm{d}s_{\boldsymbol{y}}, \qquad \boldsymbol{x}\in\Gamma_{13}, \\ S^{\Gamma_{13}}_{\rm ext}[\psi](\boldsymbol{x}) &= \int_{\Gamma_{13}} G^{k_3}_{\infty}(\boldsymbol{x},\boldsymbol{y})\psi(\boldsymbol{y})\mathrm{d}s_{\boldsymbol{y}}, \qquad \boldsymbol{x}\in\Gamma_{13}, \\ K^{\Gamma_{13}}_{\rm int}[\psi](\boldsymbol{x}) &= \int_{\Gamma_{13}} \frac{\partial G^{k_1}_{\infty}}{\partial \mathbf{n}_{\boldsymbol{x}}}(\boldsymbol{x},\boldsymbol{y})\psi(\boldsymbol{y})\mathrm{d}s_{\boldsymbol{y}}, \qquad \boldsymbol{x}\in\Gamma_{13}, \\ K^{\Gamma_{13}}_{\rm ext}[\psi](\boldsymbol{x}) &= \int_{\Gamma_{13}} \frac{\partial G^{k_3}_{\infty}}{\partial \mathbf{n}_{\boldsymbol{x}}}(\boldsymbol{x},\boldsymbol{y})\psi(\boldsymbol{y})\mathrm{d}s_{\boldsymbol{y}}, \qquad \boldsymbol{x}\in\Gamma_{13}. \end{aligned} \tag{16}$$

4. NUMERICAL METHOD

A. Discretization of Integral Equations

The integral equations (7), (11), and (15) involve either (a) integrals over $\Gamma_{13}\cup\Gamma_{24}$ with equality enforced on $\Gamma_{13}\cup\Gamma_{24}$, or (b) integrals over Γ_{13} with equality enforced on Γ_{13}. All of these integral equations can be expressed in terms of parametrizations of the curves Γ_{13} and Γ_{24}, or, more precisely, in terms of integrals of the form

$$\int_0^{2\pi} L(t,\tau)\phi(\tau)\mathrm{d}\tau \quad \text{and} \quad \int_0^{2\pi} M(t,\tau)\phi(\tau)\mathrm{d}\tau, \tag{17}$$

with kernels

$$\begin{aligned} L(t,\tau) &= G(\boldsymbol{x}(t), \quad \boldsymbol{y}(\tau))|\boldsymbol{y}'(\tau)|, \\ M(t,\tau) &= \nabla_x[G](\boldsymbol{x}(t), \quad \boldsymbol{y}(\tau)) \cdot \mathbf{n}(t)|\boldsymbol{y}'(\tau)|, \end{aligned} \tag{18}$$

where (i) each of the functions $\boldsymbol{x}(t)$ and $\boldsymbol{y}(\tau)$ denote either a parametrization for the curve Γ_{13} or of the curve Γ_{24} with parameters t and τ in the interval $(0,2\pi)$; (ii) $\mathbf{n}(t) = (x_2'(t), -x_1'(t))/|\boldsymbol{x}'(t)|$ denotes the unit normal on Γ_{13} or Γ_{24}, as appropriate, which points outward from the defect; (iii) $\phi(\tau) = \psi(\boldsymbol{y}(\tau))$, where ψ stands for the unknown density function under consideration; and iv) G denotes the relevant Green function. Indeed, in case (a) above, the integral over $\Gamma_{13}\cup\Gamma_{24}$ can be expressed as a sum of integrals on Γ_{13} and Γ_{24}. In case (b), in particular, we take $\boldsymbol{x} = \boldsymbol{y}$.

Our discretization of the integral equations (7), (11), and (15) is based on corresponding discretizations of the integrals (17). Following [27] we thus proceed by expressing the kernels (18) in the form

$$L(t,\tau) = L_1(t,\tau)\log r^2(t,\tau) + L_2(t,\tau), \tag{19a}$$

$$M(t,\tau) = M_1(t,\tau)\log r^2(t,\tau) + M_2(t,\tau), \tag{19b}$$

where L_j and M_j $(j = 1,2)$ are smooth functions on $(0,2\pi)\times(0,2\pi)$ and where $\mathbf{r}(t,\tau) = \boldsymbol{x}(t) - \boldsymbol{y}(\tau)$ and $r(t,\tau) = |\mathbf{r}(t,\tau)|$. In cases for which $\boldsymbol{x}(t)$ and $\boldsymbol{y}(\tau)$ parametrize the same open curve we have

$$\begin{aligned} L_1(t,\tau) &= -\frac{1}{4\pi}J_0(kr(t,\tau))|\boldsymbol{y}'(\tau)|, \\ L_2(t,\tau) &= L(t,\tau) - L_1(t,\tau)\log r^2(t,\tau), \\ M_1(t,\tau) &= \frac{k}{4\pi}J_1(kr(t,\tau))\mathbf{n}(t)\cdot\frac{\mathbf{r}(t,\tau)}{r}|\boldsymbol{y}'(\tau)|, \\ M_2(t,\tau) &= M(t,\tau) - M_1(t,\tau)\log r^2(t,\tau). \end{aligned}$$

The diagonal terms $L_2(t,t)$ and $M_2(t,t)$ can be computed exactly by taking the limit of $L_2(t,\tau)$ and $M_2(t,\tau)$ as $\tau \to t$ (see [27, p. 77] for details). On the other hand, when $\boldsymbol{x}(t)$ and $\boldsymbol{y}(\tau)$ parametrize different curves, L and M are smooth on $(0,2\pi)\times(0,2\pi)$ and, thus, $L_1 = 0$, $L = L_2$, $M_1 = 0$, and $M = M_2$. (Note that although in the latter case L and M are smooth functions, these functions are in fact *nearly singular*, for t near the endpoints of the parameter interval $(0,2\pi)$ for the curve $\boldsymbol{x}$, and for τ around the corresponding endpoint of the parameter interval for the curve $\boldsymbol{y}$.)

Letting K denote one of the integral kernels L or M in Eq. (19), in view of the discussion above K may be expressed in the form $K(t,\tau) = K_1(t,\tau)\log r^2(t,\tau) + K_2(t,\tau)$ for smooth kernels K_1 and K_2. For a fixed t then, there are two types of integrands for which high-order quadratures must be provided, namely integrands that are smooth in $(0,2\pi)$ but have singularities at the endpoints of the interval (that arise from corresponding singularities of the densities ϕ at the endpoints of the open curves; cf. [28–30]), and integrands that additionally have a logarithmic singularity at $\tau = t$. To handle both singular integration problems we follow [27,31] and utilize a combination of a graded meshes, the trapezoidal quadrature rule, and a quadrature rule that incorporates the logarithmic singularity into its quadrature weights—as described in what follows. Interestingly, the graded meshes and associated changes of variables give rise to accurate integration even in the near-singular regions mentioned above in this section.

To introduce graded meshes we consider the polynomial change of variables $t = w(s)$, where

$$w(s) = 2\pi\frac{[v(s)]^p}{[v(s)]^p + [v(2\pi - s)]^p}, \qquad 0 \le s \le 2\pi, \tag{20}$$

$$v(s) = \left(\frac{1}{p} - \frac{1}{2}\right)\left(\frac{\pi - s}{\pi}\right)^3 + \frac{1}{p}\frac{s-\pi}{\pi} + \frac{1}{2},$$

and where $p \ge 2$. The function w is smooth and increasing on $[0,2\pi]$, with $w^{(k)}(0) = w^{(k)}(2\pi) = 0$ for $1 \le k \le p-1$. Using this transformation we express K as

$$\begin{aligned} K(t,\tau) &= K(w(s), w(\sigma)) \\ &= K_1(w(s), w(\sigma))\log\left(4\sin^2\frac{s-\sigma}{2}\right) + \tilde{K}_2(s,\sigma), \end{aligned}$$

where

$$\begin{aligned} \tilde{K}_2(s,\sigma) = K_1(w(s), w(\sigma))\log\left(\frac{r^2(w(s), w(\sigma))}{4\sin^2\frac{s-\sigma}{2}}\right) \\ + K_2(w(s), w(\sigma)), \end{aligned}$$

and where the diagonal term is given by $\tilde{K}_2(s,\sigma) = 2K_1(t,t)\log(w'(s)|\boldsymbol{x}'(t)|) + K_2(t,t)$. High-order accurate quadrature formulae for the integral operators (17) based on the $(2n-1)$-point discretization $\sigma_j = j\pi/n$ $(1 \le j \le 2n-1$, corresponding to integration over the curve parametrized by $\boldsymbol{y}(\tau))$ at evaluation points $t = t_i = w(s_i)$ with $s_i = i\pi/q$ $(1 \le i \le 2q-1$, corresponding to evaluation of the operator at points on the curve parametrized by $\boldsymbol{x}(t))$ can easily be obtained [27] from the expressions

$$\int_0^{2\pi} f(\sigma)\mathrm{d}\sigma \approx \frac{\pi}{n}\sum_{j=0}^{2n-1} f(\sigma_j) \tag{21}$$

and

$$\int_0^{2\pi} f(\sigma)\log\left(4\sin^2\frac{s-\sigma}{2}\right)\mathrm{d}\sigma \approx \sum_{j=0}^{2n-1} R_j^{(n)}(s)f(\sigma_j),$$

$0 \le s \le 2\pi$ (which, for smooth functions f, yield high-order accuracy), where the weights $R_j(s)$ are given by

$$R_j(s) = -\frac{2\pi}{n}\sum_{m=1}^{n-1}\frac{1}{m}\cos m(s-\sigma_j) - \frac{\pi}{n^2}\cos n(s-\sigma_j).$$

Clearly setting $s = \sigma_i$ in this equation gives $R_j(\sigma_i) = R_{|i-j|}$, where

$$R_k = -\frac{2\pi}{n}\sum_{m=1}^{n-1}\frac{1}{m}\cos\frac{mk\pi}{n} - \frac{(-1)^k\pi}{n^2}.$$

Using these quadrature points and weights and corresponding parameter values $t = t_i = w(s_i)$ for the observation point $(s_i = i\pi/q)$ we obtain the desired discrete approximation for the integrals (17): for an approximation $\phi_j \approx \phi(\tau_j) = \phi(w(\sigma_j))$ we have

$$\int_0^{2\pi} K(t_i,\tau)\phi(\tau)\mathrm{d}\tau \approx \sum_{j=1}^{2n-1}\left\{K_1(t_i,\tau_j)W_{ij} + K_2(t_i,\tau_j)\frac{\pi}{n}\right\}\phi_j w'(\sigma_j) \tag{22}$$

for $1 \le i \le 2q-1$, where $\tau_j = w(\sigma_j)$ and where the quadrature weights are given by

$$W_{ij} = R_{|i-j|} + \frac{\pi}{n}\log\left(\frac{r^2(t_i,t_j)}{4\sin^2(s_i-s_j)/2}\right).$$

Note that for sufficiently large values of p the product $\phi(w(\sigma))w'(\sigma)$ [an approximation of which appears in Eq. (22)] vanishes continuously at the endpoints of the parameter interval $[0, 2\pi]$—even in cases for which, as it happens for corners or points of junction between multiple dielectric materials, $\phi(w(\sigma))$ tends to infinity at the endpoints.

The systems of boundary integral equations (7), (11), and (15) are discretized by means of applications of the quadrature rule (22) to the relevant integral operators (8), (12), and (16), respectively. This procedure leads to linear systems of algebraic equations for the unknown values of the density functions ψ_{int} and ψ_{ext} at the quadrature points. The presence of the weight $w'(\sigma_j)$ in Eq. (22), which multiplies the unknowns $\phi_j \approx \phi(\tau_j)$ and which is very small for σ_j close to 0 and 2π, however, gives rise to highly ill-conditioned linear systems. To avoid this difficulty we resort to the change of unknown $\eta_j = \phi_j w'(\sigma_j)$ in Eq. (22); for the equations that contain terms of the form $\psi_{\mathrm{int}}/2$ and $\psi_{\mathrm{ext}}/2$ it is additionally necessary to multiply both sides of the equation by $w'(\sigma_j)$ to avoid small denominators. In what follows, the resulting discrete linear systems for the problems under consideration are generically denoted by $\mathbf{A}\boldsymbol{\eta} = \mathbf{f}$, where in each case $\boldsymbol{\eta}$ is a vector that combines the unknowns that result from the discretization procedure described above in this section for the various boundary portions Γ_{ij} (cf. Fig. 2). Once $\boldsymbol{\eta}$ has been found, the numerical approximation of the scattered fields at a given point $\boldsymbol{x}$ in space, which in what follows will be denoted by $\tilde{u} = \tilde{u}(\boldsymbol{x})$, can be obtained by consideration of the relevant representation (6), (10), or (14). For evaluation points $\boldsymbol{x}$ sufficiently far from the integration curves these integrals can be accurately approximated using the change of variable $t = w(s)$ together with the trapezoidal rule (21); for observation points near the integration curves, in turn, a procedure based on interpolation along a direction transverse to the curve is used (see [32] for details).

B. Solution at Resonant and Near-Resonant Frequencies

As mentioned in Section 1, despite the fact that each one of the physical problems considered in this contribution admits unique solutions for all frequencies ω and all physically admissible values of the dielectric constant and magnetic permeability, for certain values of ω spurious resonances occur: for such values of ω the systems of integral equations derived in Section 3 are not invertible. In fact, spurious resonances for these systems arise whenever the wavenumber k_3, which will also be denoted by κ in what follows, is such that $-k_3^2 = -\kappa^2$ equals a certain Dirichlet eigenvalue. (More precisely, letting $\varepsilon(x)$ and $\mu(x)$ denote the prescribed (piecewise constant) permittivity and permeability, spurious resonances occur whenever κ satisfies $\Delta u = -\kappa^2\varepsilon(x)\mu(x)u$ in $\Omega_1 \cup \Omega_2$ for some nonzero function u satisfying $u = 0$ on $\partial(\Omega_1 \cup \Omega_2)$. This can be established, e.g., taking into account ideas underlying uniqueness arguments of the type found in [33, Chap. 3]. Note, in particular, that the values of κ for which spurious resonances occur are necessarily real numbers (and, thus, physically realizable), since the eigenvalues $-\kappa^2$ are necessarily negative.)

It is important to note that, in addition to the spurious resonances mentioned above, the transmission problems considered in Section 2 *themselves* (and, therefore the corresponding systems of integral equations mentioned above) also suffer from nonuniqueness for certain *nonphysical* values of κ ($\Im(\kappa) < 0$), which are known as "scattering poles" [34]; cf. Fig. 4 and a related discussion below in this section.

The noninvertibility of the aforementioned continuous systems of integral equations at a spurious-resonance or scattering-pole wavenumber $\kappa = \kappa^*$ manifests itself at the discrete level in noninvertibility or ill-conditioning of the system matrix $\mathbf{A} := \mathbf{A}(\kappa)$ for values of κ close to κ^*. Therefore, for κ near κ^* the numerical solution of the transmission problems under consideration (which in what follows will be denoted by $\tilde{u} := \tilde{u}_\kappa(\boldsymbol{x})$ to make explicit the solution dependence on the parameter κ) cannot be obtained via direct solution of the linear system $\mathbf{A}\boldsymbol{\eta} = \mathbf{f}$. As is known, however [34], the solutions $u = u_\kappa$ of the continuous transmission problems are analytic functions of κ for all real values of κ—including, in particular, for κ equal to any one of the spurious resonances mentioned above and for real values of κ near a scattering pole—and therefore, the approximate values $\tilde{u}_\kappa(\boldsymbol{x})$ for κ sufficiently far from κ^* can be used, via analytic continuation, to obtain corresponding approximations around $\kappa = \kappa^*$ and even at a spurious resonance $\kappa = \kappa^*$.

In order to implement this strategy for a given value of κ it is necessary for our algorithm to possess the capability to perform two main tasks, namely, Task I—determination of whether κ is "sufficiently far" from any one of the spurious resonances and scattering poles κ^*— and Task II—evaluation of analytic continuations to a given real wavenumber κ_0 that is either close or equal to a spurious resonance κ^*, or that lies close to a scattering pole κ^*. Once these capabilities are available the algorithm can be completed readily: if completion of Task I leads to the conclusion that κ is far from all spurious resonances, then the solution process proceeds directly via solution of the associated system of integral equations. Otherwise, the solution process is completed by carrying out Task II. Descriptions of the proposed methodologies to perform Tasks I and II are presented in the following two sections.

1. Task I: Matrix-Singularity Detection

Consider a given wavenumber κ' for which a solution to one of the problems under consideration needs to be obtained. As discussed in what follows, in order to determine the level of proximity of κ' to a spurious resonance or scattering pole κ^*, the matrix-singularity detection algorithm utilizes the minimum singular value $\sigma_{\min}(\kappa')$ of $\mathbf{A}(\kappa')$. (Note that in view of the

discussion concerning Task I above in the present Section 4.B it is not necessary to distinguish wavenumbers κ' that lie near to either a spurious resonance or a scattering pole: both cases can be treated equally well by means of one and the same Task II (analytic-continuation) algorithm (Section 4.B.2).

To introduce the matrix-singularity detection algorithm consider Fig. 3: clearly, except for a sequence of wavenumbers (spurious resonances and/or real wavenumbers close to nonreal scattering pole) around which the minimum singular value is small, the function $\sigma_{\min}(\kappa)$ maintains an essentially constant level. This property forms the basis of the matrix-singularity detection algorithm. Indeed, noting that there are no singularities for κ smaller than certain threshold (as it follows from the spectral theory for the Laplace operator), we choose a wavenumber $\kappa_0 > 0$ close to zero and we compare $\sigma_{\min}(\kappa_0)$ with $\sigma_{\min}(\kappa')$. If $\sigma_{\min}(\kappa') \ll \sigma_{\min}(\kappa_0)$, say $\sigma_{\min}(\kappa') < \xi \cdot \sigma_{\min}(\kappa_0)$ for an adequately chosen value of ξ, κ' is determined to be close to some singularity κ^*, and therefore the Task-II analytic-continuation algorithm is utilized to evaluate $\tilde{u}_{\kappa'}(\boldsymbol{x})$. The parameter values $\kappa_0 = 0.1$ and $\xi = 10^{-4}$ were used in all the numerical examples presented in this paper.

(A remark is in order concerning the manifestations of resonances and scattering poles on the plots of the function $\sigma_{\min}(\kappa)$ as a function of the real variable κ. By definition the function $\sigma_{\min}(\kappa)$ vanishes exactly at all spurious resonances. The four sharp peaks shown in Fig. 3, for example, occur at the spurious resonances listed in the inset of Fig. 4. The first peak from the left in Fig. 3, in contrast, is not sharp—as can be seen in the inset close-up included in the figure. The small value $\sigma_{\min}(\kappa) \sim 10^{-7}$ around $\kappa = 0.5708$ is explained by the presence of a scattering pole κ^*: $\sigma_{\min}(\kappa^*) = 0$ at the complex wavenumber $\kappa^* = 0.57807113743881 - 0.000074213015953i$. Thus scattering poles can in practice be quite close to the real κ axis, and thus give rise to rather sharp peaks that are not associated with actual spurious resonances. As mentioned above, however, the analytic-continuation algorithm presented in what follows need not differentiate between these two types of singularities: analytic continuation is utilized whenever a sufficiently small value of $\sigma_{\min}$ is detected.)

2. Task II: Analytic Continuation

Analytic continuation of the numerical solution $\tilde{u}_{\kappa}(\boldsymbol{x})$ to a given wavenumber κ' detected as a matrix singularity

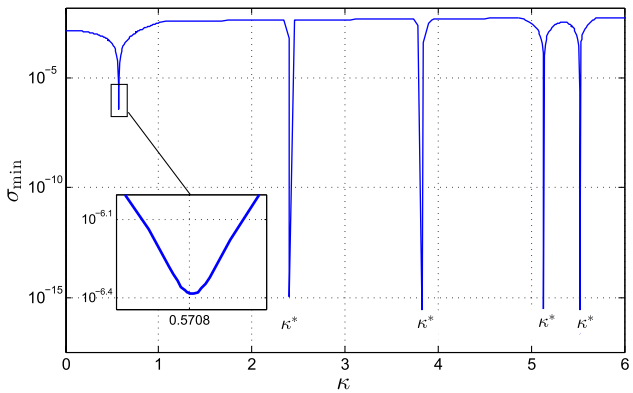

Fig. 3. Minimum singular value of $\mathbf{A}$ as a function of $\kappa = k_3$ for the problem of scattering by a semicircular bump on a PEC half-plane in TE polarization.

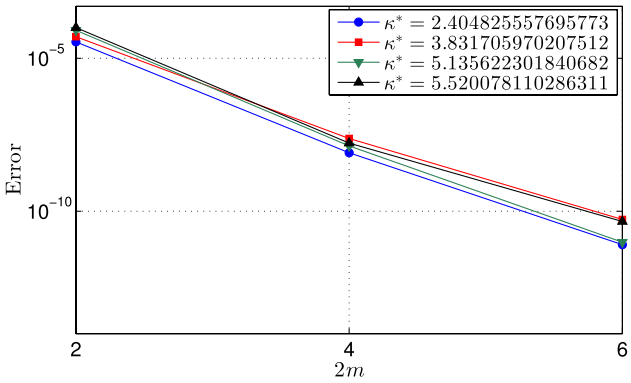

Fig. 4. Error in the approximation of $\tilde{u}_{\kappa^*}$ by Chebyshev interpolation/analytic continuation for various spurious resonant frequencies κ^* as a function of the order $2m$ of the Chebyshev expansion.

(Section 4.B.1) is carried out via interpolation. Note, however, that, since $\mathbf{A}(\kappa)$ is generally extremely ill-conditioned for values of κ in a narrow interval around such wavenumbers κ', fine interpolation meshes cannot be utilized to achieve arbitrary accuracy in the approximation. To overcome this difficulty we utilize an interpolation method based on use of Chebyshev expansions, for which the meshsize is not allowed to be smaller than a certain tolerance, and within which convergence is achieved, in view of the analyticity of the scattered field with respect to the wavenumber κ, by increasing the order of the Chebyshev expansion. To do this for a given wavenumber κ' identified by the matrix-singularity detection algorithm (Section 4.B.1), the analytic-continuation algorithm proceeds by introducing a Chebyshev grid of points $\{\kappa_j\}_{j=1}^{2m}$ (cf. [35]) sorted in ascending order such that the two middle points in the grid, κ_m and κ_{m+1}, lie at an appropriately selected distance $\delta > 0$ from the wavenumber κ': $\kappa_m = \kappa' - \delta$ and $\kappa_{m+1} = \kappa' + \delta$.

The accuracy of the numerical evaluation of the field $\tilde{u}_{\kappa_j}$ at each one of the interpolation points κ_j is ensured by running the matrix-singularity detection algorithm at each κ_j and adequately changing the value of δ if a matrix singularity is detected at one or more of the mesh points κ_j. Letting $\tilde{u}_{\kappa}^{(m)}$ denote the Chebyshev expansion of order $2m-1$ resulting for a Chebyshev mesh selected as indicated above, the sequence $\tilde{u}_{\kappa'}^{(m)}$ convergences exponentially fast to $\tilde{u}_{\kappa'}$ as m grows—as it befits Chebyshev expansions of analytic functions. If the matrix-singularity condition $\sigma_{\min}(\kappa_{j_\ell}) < \xi \cdot \sigma_{\min}(\kappa_0)$ occurs at one of more of the interpolation points κ_j, say κ_{j_ℓ}, $1 \le \ell \le L'$, the algorithm proceeds by selecting the smallest value of the parameter $\delta' > \delta$ and a new set of Chebyshev points $\{\kappa'_j\}_{j=1}^{2m'}$ $(m' \ge m)$ satisfying $\kappa'_{m'} = \kappa' - \delta'$, $\kappa'_{m'+1} = \kappa' + \delta'$, such that none of the new interpolation points lie on the region $\bigcup_{\ell=1}^{L'}(\kappa_{j_\ell} - \delta, \kappa_{j_\ell} + \delta)$. If the condition $\sigma_{\min}(\kappa'_j) < \xi \cdot \sigma_{\min}(\kappa_0)$ occurs for some of the new interpolation points, say κ'_{j_ℓ}, $1 \le \ell \le L''$, the algorithm proceeds as described above, but for a new value $\delta'' > \delta'$, and so on. Note that in practice the interpolation procedure described above is rarely needed, and when it is needed, a suitable interpolation grid is usually found after a single iteration: in practice the choice $\delta = 0.01$ has given excellent results in all the examples presented in this paper.

Table 1. Convergence Test for the Numerical Solution of Problem Type I ($k_1 = 5$, $k_2 = 15$ or $15 + 5i$, $k_3 = 5$, and $k_4 = 7$), II ($k_1 = 5$, $k_2 = 15$, or $15 + 5i$, and $k_3 = 5$), and III ($k_1 = 15$ or $15 + 5i$, and $k_3 = 5$)

		Type I		Type II		Type III	
		k_2		k_2		k_1	
	P	15	$15 + 5i$	15	$15 + 5i$	15	$15 + 5i$
TM	63	$3 \cdot 10^{-01}$	$6 \cdot 10^{-03}$	$7 \cdot 10^{-01}$	$1 \cdot 10^{-04}$	$2 \cdot 10^{-01}$	$7 \cdot 10^{-02}$
	127	$7 \cdot 10^{-04}$	$4 \cdot 10^{-06}$	$2 \cdot 10^{-03}$	$1 \cdot 10^{-07}$	$2 \cdot 10^{-03}$	$1 \cdot 10^{-03}$
	255	$1 \cdot 10^{-10}$	$7 \cdot 10^{-12}$	$3 \cdot 10^{-11}$	$6 \cdot 10^{-12}$	$5 \cdot 10^{-08}$	$8 \cdot 10^{-08}$
	511	$6 \cdot 10^{-12}$	$5 \cdot 10^{-12}$	$1 \cdot 10^{-12}$	$3 \cdot 10^{-13}$	$1 \cdot 10^{-13}$	$8 \cdot 10^{-13}$
TE	63	$9 \cdot 10^{-02}$	$3 \cdot 10^{-03}$	$2 \cdot 10^{-01}$	$6 \cdot 10^{-04}$	$4 \cdot 10^{-01}$	$4 \cdot 10^{-02}$
	127	$3 \cdot 10^{-04}$	$7 \cdot 10^{-06}$	$1 \cdot 10^{-04}$	$2 \cdot 10^{-07}$	$1 \cdot 10^{-03}$	$3 \cdot 10^{-04}$
	255	$3 \cdot 10^{-12}$	$2 \cdot 10^{-12}$	$3 \cdot 10^{-12}$	$7 \cdot 10^{-12}$	$2 \cdot 10^{-08}$	$2 \cdot 10^{-08}$
	511	$1 \cdot 10^{-12}$	$2 \cdot 10^{-12}$	$4 \cdot 10^{-14}$	$1 \cdot 10^{-14}$	$1 \cdot 10^{-13}$	$2 \cdot 10^{-13}$

In order to demonstrate the fast convergence of $\tilde{u}^{(m)}_{\kappa'}$ to $\tilde{u}_{\kappa'}$ as m increases, we consider the problem of scattering by a dielectric unit-radius semicircular bump on a PEC half-plane. For this problem the wavenumbers κ^* for which the system of integral equations (15) is noninvertible can be computed explicitly: spurious resonances are given by real solutions of the equation $J_n(\kappa) = 0$, $n \geq 0$, where J_n denotes the Bessel function of first kind and order n, and scattering poles are complex valued solutions of $\kappa H^{(1)}_n(\kappa) J'_n(k_1) = k_1 J_n(k_1) H^{(1)\prime}_n(\kappa)$, where $H^{(1)}_n$ denotes the Hankel function of first kind and order n (see [26]). The function $\sigma_{\min}(\kappa)$ is displayed in Fig. 3. The κ^* values identified in that figure coincide (up to machine precision) with the first four positive solutions of the equation $J_n(\kappa) = 0$. On the other hand, this problem admits an analytical solution u_κ in terms of a Fourier–Bessel expansion (see [26]). The availability of the exact solution allows us to quantify the magnitude of interpolation error by evaluating the maximum of the error function $E(\boldsymbol{x}) = |\tilde{u}^{(m)}_{\kappa^*}(\boldsymbol{x}) - u_{\kappa^*}(\boldsymbol{x})|$ at a polar grid Π (consisting of points inside, outside, and at the boundary of the semicircular bump). Figure 4 shows the error $\max_{\boldsymbol{x}\in\Pi} E(\boldsymbol{x})$ versus the number of points used in the Chebyshev interpolation of $\tilde{u}_{\kappa^*}$, which is computed for the four spurious resonances k^* shown in Fig. 3, and where a sufficiently fine spatial discretization is used. In all the calculations $k_1 = 6$, the curve Γ_{13} is discretized using 128 points, and $\delta = 0.01$ is utilized to construct the Chebyshev grids.

5. NUMERICAL RESULTS

This section demonstrates the high accuracies and high-order convergence that result as the proposed boundary integral methods are applied to each one of the mathematical problems formulated in Section 3. For definiteness all dielectric media are assumed nonmagnetic so that $\beta_i/\beta_j = 1$ for TM polarization and $\beta_i/\beta_j = k_i^2/k_j^2$ for TE polarization. In all the numerical examples shown in this section the incident plane wave is parallel to the vector $d = (\cos(\pi/3), -\sin(\pi/3))$ and the graded-mesh parameter (20) is $p = 8$.

We thus consider the problem of scattering by a dielectric-filled cavity on a dielectric half-plane (Problem Type I), the problem of scattering by a dielectric-filled cavity on a PEC half-plane (Problem Type II), and the problem of scattering by a dielectric bump on a PEC half-plane (Problem Type III). With reference to Fig. 2, in the first two examples the cavity is determined by the curve $\Gamma_{24} = \{(x,y) \in \mathbb{R}^2 : x = -\cos(t/2), y = (\cos(4t)/40)t(t-2\pi) - \sin(t/2), t \in (0,2\pi)\}$, and the curve Γ_{13} (which, in view of the formulation in Section 3, may be selected rather arbitrarily as long as it lies in the upper half-plane and has the same endpoints as Γ_{24}) is given by the semicircle of radius one in the upper half-plane that joins the points (1,0) and (−1, 0). For the problem of scattering by a dielectric bump (Type III problem), in turn, the boundary of the bump is given by $\Gamma_{13} = \{(x,y) \in \mathbb{R}^2 : x = \cos(t/2), y = (\cos(4t)/40)t(2\pi - t) + \sin(t/2), t \in (0,2\pi)\}$.

To estimate the error in the aforementioned numerical test problems, the systems of boundary integral equations (7), (11), and (15) were discretized utilizing five different meshes Π_j, $1 \leq j \leq 5$ consisting of $P = 2^{j+5} - 1$ points distributed along each of the relevant boundaries: P points on Γ_{24} and P points on Γ_{13} in the case of Type I and II problems, and P points on Γ_{13} in the case of the Type III problem.

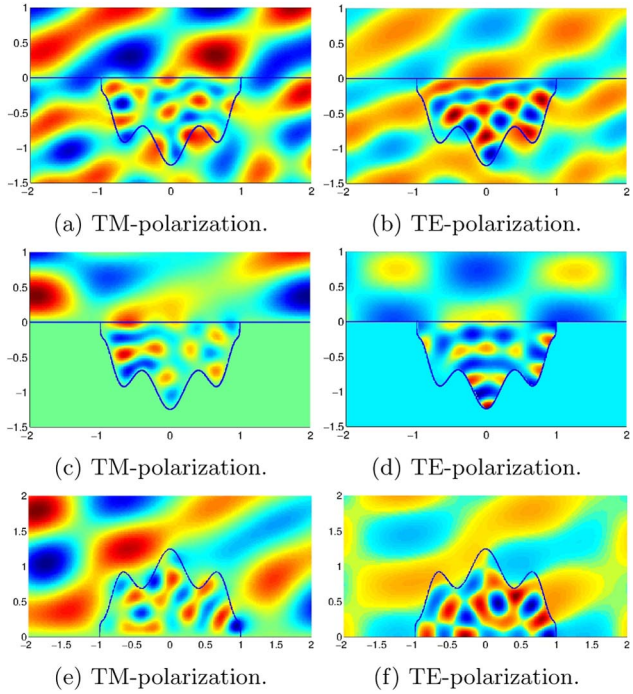

(a) TM-polarization. (b) TE-polarization.
(c) TM-polarization. (d) TE-polarization.
(e) TM-polarization. (f) TE-polarization.

Fig. 5. Diffraction pattern resulting from the scattering of a plane wave by (a), (b) dielectric-filled cavity on a dielectric half-plane, (c), (d) dielectric-filled cavity on a PEC half-plane, and (e), (f) dielectric bump on a PEC half-plane.

The sequence of meshes is chosen to be nested ($\Pi_j \subset \Pi_i$ for $j < i$) in order to facilitate the convergence analysis; in what follows the numerical solution that results from the discretization Π_j is denoted by $\tilde{u}_j$. The error in the numerical solution $\tilde{u}_j$ is estimated by means of the expression

$$E_j = \frac{\max_{x\in\Pi_1}|\tilde{u}_j(x) - \tilde{u}_5(x)|}{\max_{x\in\Pi_1}|\tilde{u}_5(x)|}, \qquad 1 \le j \le 4.$$

Table 1 presents the numerical error estimates E_j, $1 \le j \le 5$, for the three different problem types (including real and complex wavenumbers); clearly high accuracies and fast convergence are achieved in all cases. To further illustrate the results provided by the proposed method, the real part of the total field is presented in Fig. 5 for some of the cases considered in this section, including examples for TM and TE polarization. Thus, Figs. 5(a) and 5(b) present the diffraction pattern for the problem of scattering by the dielectric-filled cavity on the dielectric half-plane (problem Type I) with wavenumbers $k_2 = 15$, $k_1 = k_3 = 5$, and $k_4 = 7$; Figs. 5(c) and 5(d) present the diffraction pattern for the problem of scattering by the dielectric-filled cavity on the PEC half-plane (problem Type II) with $k_2 = 15$ and $k_1 = k_3 = 5$; and Figs. 5(e) and 5(f) present the diffraction pattern for the problem of scattering by the dielectric bump on the PEC half-plane for $k_1 = 15$ and $k_3 = 5$.

ACKNOWLEDGMENTS

The authors gratefully acknowledge support from the Air Force Office of Scientific Research and the National Science Foundation.

REFERENCES

1. R. Ruppin, "Electric field enhancement near a surface bump," Solid State Commun. **39**, 903–906 (1981).
2. P. Zhang, Y. Y. Lau, and R. M. Gilgenbach, "Analysis of radio-frequency absorption and electric and magnetic field enhancements due to surface roughness," J. Appl. Phys. **105**, 1–9 (2009).
3. B. Alavikia and O. M. Ramahi, "Hybrid finite element-boundary integral algorithm to solve the problem of scattering from a finite array of cavities with multilayer stratified dielectric coating," J. Opt. Soc. Am. A **28**, 2192–2199 (2011).
4. Rayleigh, "On the light dispersed from fine lines ruled upon reflecting surfaces or transmitted by very narrow slits," Philos. Mag. Series **14**(81), 350–359 (1907).
5. W. J. Byun, J. W. Yu, and N. H. Myung, "TM scattering from hollow and dielectric-filled semielliptic channels with arbitrary eccentricity in a perfectly conducting plane," IEEE Trans. Microwave Theory Tech. **46**, 1336–1339 (1998).
6. H. Eom and G. Hur, "Gaussian beam scattering from a semicircular boss above a conducting plane," IEEE Trans. Antennas Propag. **41**, 106–108 (1993).
7. S. J. Lee, D. J. Lee, W. S. Lee, and J. W. Yu, "Electromagnetic scattering from both finite semi-circular channels and bosses in a conducting plane: TM case," J. Electromagn. Waves Appl. **26**, 2398–2409 (2012).
8. T. Park, H. Eom, and K. Yoshitomi, "Analysis of TM scattering from finite rectangular grooves in a conducting plane," J. Opt. Soc. Am. A **10**, 905–911 (1993).
9. T. J. Park, H. J. Eom, Y. Yamaguchi, and W.-M. Boerner, "TE-plane wave scattering from a trough in a conducting plane," J. Electromagn. Waves Appl. **7**, 235–245 (1993).
10. A. Tyzhnenko, "Two-dimensional TE-plane wave scattering by a dielectric-loaded semicircular trough in a ground plane," Electromagnetics **24**, 357–368 (2004).
11. A. G. Tyzhnenko, "A unique solution to the 2-d H-scattering problem for a semicircular trough in a PEC ground plane," Prog. Electromagn. Res. **54**, 303–319 (2005).
12. J.-W. Yu, W. J. Byun, and N.-H. Myung, "Multiple scattering from two dielectric-filled semi-circular channels in a conducting plane: TM case," IEEE Trans. Antennas Propag. **50**, 1250–1253 (2002).
13. M. Basha, S. Chaudhuri, S. Safavi-Naeini, and H. Eom, "Rigorous formulation for electromagnetic plane-wave scattering from a general-shaped groove in a perfectly conducting plane," J. Opt. Soc. Am. A **24**, 1647–1655 (2007).
14. M. K. Hinders and A. D. Yaghjian, "Dual-series solution to scattering from a semicircular channel in a ground plane," IEEE Microwave Guided Wave Lett. **1**, 239–242 (1991).
15. B. K. Sachdeva and R. A. Hurd, "Scattering by a dielectric loaded trough in a conducting plane," J. Appl. Phys. **48**, 1473–1476 (1977).
16. B. Alavikia and O. M. Ramahi, "Finite-element solution of the problem of scattering from cavities in metallic screens using the surface integral equation as a boundary constraint," J. Opt. Soc. Am. A **26**, 1915–1925 (2009).
17. G. Bao and W. Sun, "A fast algorithm for the electromagnetic scattering from a large cavity," SIAM J. Sci. Comput. **27**, 553–574 (2005).
18. K. Du, "Two transparent boundary conditions for the electromagnetic scattering from two-dimensional overfilled cavities," J. Comput. Phys. **230**, 5822–5835 (2011).
19. P. Li and A. Wood, "A two-dimensional Helmhotlz equation solution for the multiple cavity scattering problem," J. Comput. Phys. **240**, 100–120 (2013).
20. T. Van and A. Wood, "Finite element analysis of electromagnetic scattering from a cavity," IEEE Trans. Antennas Propag. **51**, 130–137 (2003).
21. Y. Wang, K. Du, and W. Sun, "A second-order method for the electromagnetic scattering from a large cavity," Numer. Math. Theory Methods Appl. **1**, 357–382 (2008).
22. A. Wood, "Analysis of electromagnetic scattering from an overfilled cavity in the ground plane," J. Comput. Phys. **215**, 630–641 (2006).
23. E. Howe and A. Wood, "TE solutions of an integral equations method for electromagnetic scattering from a 2D cavity," IEEE Antennas Wirel. Propag. Lett. **2**, 93–96 (2003).
24. C.-F. Wang and Y.-B. Gan, "2D cavity modeling using method of moments and iterative solvers," Prog. Electromagn. Res. **43**, 123–142 (2003).
25. W. D. Wood and A. W. Wood, "Development and numerical solution of integral equations for electromagnetic scattering from a trough in a ground plane," IEEE Trans. Antennas Propag. **47**, 1318–1322 (1999).
26. C. Pérez-Arancibia and O. P. Bruno, "High-order integral equation methods for problems of scattering by bumps and cavities on half-planes," arXiv:1405.4336 (2014).
27. D. Colton and R. Kress, *Inverse Acoustic and Electromagnetic Scattering Theory*, 3rd ed. (Springer, 2012), Vol. **93**.
28. O. P. Bruno, J. S. Ovall, and C. Turc, "A high-order integral algorithm for highly singular PDE solutions in Lipschitz domains," Computing **84**, 149–181 (2009).
29. J. Meixner, "The behavior of electromagnetic fields at edges," IEEE Trans. Antennas Propag. **20**, 442–446 (1972).
30. J. Van Bladel, "Field singularities at metal-dielectric wedges," IEEE Trans. Antennas Propag. **33**, 450–455 (1985).
31. R. Kress, "A Nystrom method for boundary integral equations in domains with corners," Numer. Math. **58**, 145–161 (1990).
32. E. Akhmetgaliyev and O. P. Bruno are preparing a manuscript to be called "A boundary integral strategy for the Laplace Dirichlet/Neumann mixed eigenvalue problem."
33. D. L. Colton and R. Kress, *Integral Equation Methods in Scattering Theory*, 1st ed., Pure and Applied Mathematics (Wiley, 1983).
34. M. Taylor, *Partial Differential Equations II: Qualitative Studies of Linear Equations*, Vol. **117** of Applied Mathematical Sciences (Springer, 1996).
35. E. Isaacson and H. Keller, *Analysis of Numerical Methods* (Dover, 1994).